THE JOURNAL OF PHYSICAL CHEMISTRY B LETTERS

2006, *110,* 1516−1519
Published on Web 01/10/2006

Fabrication and Photoluminescent Properties of Heteroepitaxial ZnO/$Zn_{0.8}Mg_{0.2}O$ Coaxial Nanorod Heterostructures

Won Il Park, Jinkyoung Yoo, Dong-Wook Kim, and Gyu-Chul Yi*

National CRI Center for Semiconductor Nanorods and Department of Materials Science and Engineering, Pohang University of Science and Technology (POSTECH), Pohang 790-784, Korea

Miyoung Kim

School of Materials Science & Engineering, College of Engineering, Seoul National University, Seoul 151-744, Korea

Received: July 22, 2005; In Final Form: October 20, 2005

ZnO/$Zn_{0.8}Mg_{0.2}O$ coaxial nanorod heterostructures were prepared by employing catalyst-free metal−organic vapor-phase epitaxy, and their structural and photoluminescent (PL) properties were investigated using transmission electron microscopy (TEM) and temperature-dependent PL spectroscopy. TEM images show that $Zn_{0.8}Mg_{0.2}O$ layers were epitaxially grown on the entire surfaces of the ZnO nanorods and the ZnO nanorod diameters as a core material were as small as 9 ± 2 nm. A dominant PL peak was observed at 3.316 eV, from room-temperature PL spectra of ZnO/$Zn_{0.8}Mg_{0.2}O$ coaxial nanorod heterostructures with ZnO core diameters of 9 nm, indicating a PL blue shift of 30 meV, which resulted from a quantum confinement effect along the radial direction in ZnO nanorods. Furthermore, temperature-dependent PL properties of the coaxial nanorod heterostructures were investigated, showing much higher PL intensity for the coaxial nanorod heterostructures than that of bare ZnO nanorods at room temperature. The origin of the enhanced PL intensity and reduced thermal quenching for the coaxial nanorod heterostructures is also discussed.

One-dimensional (1D) nanorod heterostructures which show composition modulation along the axial[1−5] or radial[6,7] direction have been fashioned into versatile building blocks for many electronic and photonic nanodevice applications. For instance, if a shell layer in a coaxial nanorod heterostructure has a wider band gap energy and a lower refractive index than a core layer, confinement of both carriers and photons in the core nanorod is significantly enhanced, which enables fabrication of highly efficient light-emitting devices, as already proven for quantum well or quantum wire semiconductor lasers.[8] In addition, low-dimensional carrier gas is formed for coaxial nanorod heterostructures with abrupt interfaces, essential for the fabrication of nanometer-scale transistors with high carrier mobility.[6] Nevertheless, a rational synthetic strategy for 1D heterostructures, which can fulfill various application requirements, is not yet fully established. Although 1D coaxial nanowire heterostructures including GaN/(Al, Ga)N[9] and ZnO/(Mg, Zn)O[10] have recently been fabricated by the vapor−liquid−solid (VLS) process, a clean and abrupt interface has not been produced, presumably because of spontaneous phase separation inducing self-ordered formation of coaxial heterostructures. In particular, difficulties with thickness and composition controls of the each layer hinders us from synthesizing artificial heterojunction structures. These exciting challenges in overcoming such problems inspire us to facilitate sophisticated metal−organic vapor-phase epitaxy (MOVPE) for attaining accurate layer thickness and composition controls of coaxial nanorod heterostructures and to further explore quantum confinement in novel coaxial nanorod heterostructures. Here, we report fabrication of heteroepitaxial ZnO/ZnMgO coaxial nanorod heterostructures by MOVPE and their photoluminescent characteristics.

ZnO/$Zn_{1-x}Mg_xO$ coaxial nanorod heterostructures were synthesized by in situ heteroepitaxial growth of a $Zn_{1-x}Mg_xO$ thin layer on ZnO core nanorods. MOVPE was employed for the fabrication of $Zn_{1-x}Mg_xO$/ZnO coaxial nanorods with an abrupt interface, homogeneous compositions, and a uniform layer thickness.[11] We employed a two-step MOVPE process consisting of (i) high-temperature synthesis of ultrafine core ZnO nanorods and (ii) subsequent low-temperature $Zn_{1-x}Mg_xO$ shell layers coated on core ZnO to fabricate the ZnO/$Zn_{1-x}Mg_xO$ coaxial nanorod heterostructures, as schematically shown in Figure 1a. As an initial step, core ultrafine ZnO nanorods were prepared at 800−900 °C using diethylzinc (DEZn) and oxygen as the reactants, with argon as the carrier gas. Nanorod diameters determined by electron microscopy images were as small as 9 nm with a normalized standard deviation value (a standard deviation divided by a mean) of 0.2−0.3. Detailed synthesis of ultrafine ZnO nanorods is reported elsewhere.[12] Subsequent depositions of $Zn_{1-x}Mg_xO$ shell layers were in situ performed at low temperatures of 450−550 °C by the addition of bis(cyclopentadienyl)Mg (cp_2Mg) as the Mg precursor in the same chamber, resulting in a $Zn_{1-x}Mg_xO$ layer coating all ZnO nanorod surfaces. The Mg content and thickness in $Zn_{1-x}Mg_xO$ layers were easily controlled by changing the cp_2Mg flow rate

* Corresponding author. Email: gcyi@postech.ac.kr.

10.1021/jp054066y CCC: $33.50

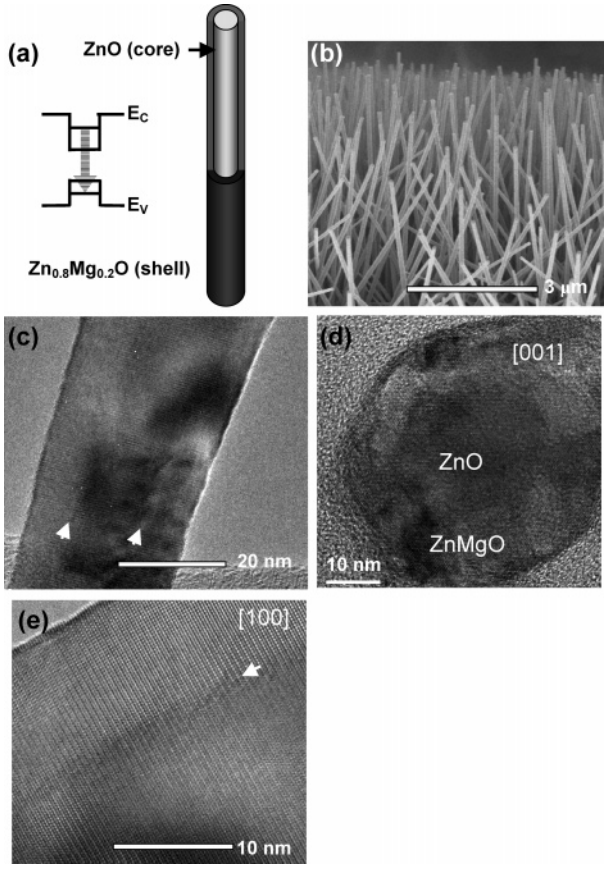

Figure 1. (a) Schematic and (b−e) electron microscopy images of ZnO/$Zn_{0.8}Mg_{0.2}O$ coaxial nanorod heterostructures. (b) Typical FE-SEM images of ZnO/$Zn_{0.8}Mg_{0.2}O$ coaxial nanorod heterostructures. TEM images of ZnO/$Zn_{0.8}Mg_{0.2}O$ coaxial nanorod heterostructures measured along (c) longitudinal and (d) transverse (cross-sectional) directions. The cross-sectional TEM image of the ZnO/$Zn_{0.8}Mg_{0.2}O$ coaxial nanorod heterostructure exhibits well-developed {10−10} facets in the ZnO core with an abrupt interface between ZnO and $Zn_{0.8}Mg_{0.2}O$. (e) HR-TEM image of ZnO/$Zn_{0.8}Mg_{0.2}O$ coaxial nanorod heterostructures. From the HR-TEM measurements, lattice images of the nanorod heterostructures without any visible defect formation were clearly observed.

and growth time, respectively. The $Zn_{1-x}Mg_xO$ shell layer coating on the ultrafine ZnO nanorods was robust and was not peeled off.

Field-emission transmission electron microscopy (FE-TEM) (Philips 300 kV) with 1.7 Å point resolution was used for structural characterizations of ZnO/$Zn_{1-x}Mg_xO$ coaxial nanorod heterostructures. The average concentration of Mg in the $Zn_{1-x}Mg_xO$ layers studied in this research was 20 atom % as determined by energy-dispersive X-ray spectroscopy in the TEM column. For further structural characterizations, synchrotron X-ray diffraction (SR-XRD) measurements of ZnO/$Zn_{0.8}Mg_{0.2}O$ nanorod heterostructures were also performed at the X-ray wavelength of 1.305 Å in the 8C2 high-resolution powder diffraction beamline at the Pohang Accelerator Laboratory. In addition, photoluminescence (PL) measurements were performed using a He−Cd laser (λ = 325 nm) as an excitation source. Details of the PL measurements are described elsewhere.[13]

Figure 1b shows a typical field-emission scanning electron microscopy (FE-SEM) image of ZnO/$Zn_{0.8}Mg_{0.2}O$ coaxial nanorod heterostructures. In comparison with bare ZnO nanorods, there is no significant change in the morphology, except that nanorod diameters increased with $Zn_{0.8}Mg_{0.2}O$ shell coating time. As shown in Figure 1c,d, furthermore, HR-TEM images were obtained by TEM measurements of the nanorod heterostructures along longitudinal and transverse (cross-sectional) directions of the nanorods, which clearly revealed the formation of ZnO/$Zn_{0.8}Mg_{0.2}O$ coaxial nanorod heterostructures by the contrast change due to the composition difference between core and shell layers along the radial direction. For the transverse directional TEM measurements, the coaxial nanorod heterostructures were sliced. perpendicular to the *c*-axis of the nanorods using an ultramicrotome. The cross-sectional TEM image of the ZnO/$Zn_{0.8}Mg_{0.2}O$ coaxial nanorod heterostructure exhibits well-developed {10−10} facets in the ZnO core with an abrupt interface between ZnO and $Zn_{0.8}Mg_{0.2}O$. These TEM images indicate that the $Zn_{0.8}Mg_{0.2}O$ shell layers with a thickness of 11−14 nm covered the entire surfaces of the ZnO core nanorod continuously and uniformly. On the basis of the shell layer thickness measurements by both TEM and SEM, the coating rate was estimated to be 3.2 nm/min.

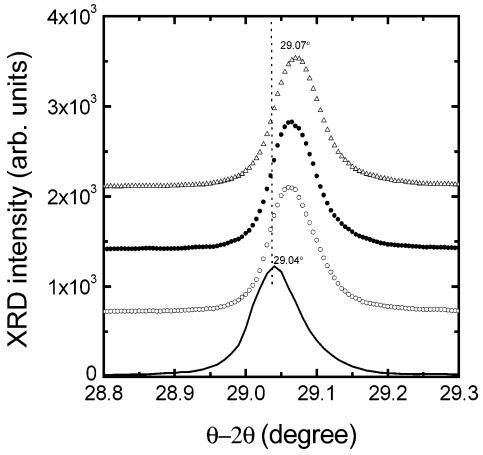

Figure 2. SR-XRD patterns of ultrafine ZnO and ZnO/$Zn_{0.8}Mg_{0.2}O$ coaxial nanorod heterostructures with different $Zn_{0.8}Mg_{0.2}O$ shell layer thicknesses of 4−13 nm.

The HR-TEM image also shows very clean and abrupt interfaces between the ZnO and $Zn_{0.8}Mg_{0.2}O$ layers as indicated by arrows in the TEM images. Apart from the difference in TEM image contrast, the lattice images of both layers were hardly distinguishable, and the interface was not easily recognizable, as shown in Figure 1e. Dislocations at the interfaces or at the shell layer were rarely observed, as little as at the bare ZnO layer, while dislocations were quite often observed for lattice-mismatched GaN/ZnO coaxial nanorod heterostructures.[14] The electronic structure observed from the electron energy-loss spectrometer also showed little difference in the conduction band structure of the oxygen K edge at the ZnO and $Zn_{0.8}Mg_{0.2}O$ layers.[15] These TEM results strongly suggest that the growth of $Zn_{0.8}Mg_{0.2}O$ on ZnO is coherently epitaxial, presumably resulting from the small lattice mismatch between the ZnO and $Zn_{0.8}Mg_{0.2}O$ layers of less than 0.5%.

Figure 2 shows SR-XRD $\theta-2\theta$ scan results of ZnO nanorods and ZnO/$Zn_{0.8}Mg_{0.2}O$ coaxial nanorod heterostructures. While a dominant peak was observed at 29.04° from the SR-XRD $\theta-2\theta$ scan data of the ZnO nanorods, corresponding to ZnO-(00·2), a $Zn_{0.8}Mg_{0.2}O$ layer coating ZnO nanorods resulted in shifting XRD peaks to a higher angle with a slight increase in its full width at half-maximum value, depending on the $Zn_{0.8}Mg_{0.2}O$ layer thickness. Furthermore, ZnO/$Zn_{0.8}Mg_{0.2}O$ coaxial nanorod heterostructures with $Zn_{0.8}Mg_{0.2}O$ layer thicknesses of 4, 6, and 13 nm show SR-XRD peak shifts to 29.05°, 29.06°, and 29.07°, respectively. The peak shift in the XRD curves originates from difference between ZnO and $Zn_{0.8}Mg_{0.2}O$ lattice constants. Although this peak shift indicates a lattice strain between ZnO and $Zn_{0.8}Mg_{0.2}O$ layers, epitaxial growth of the

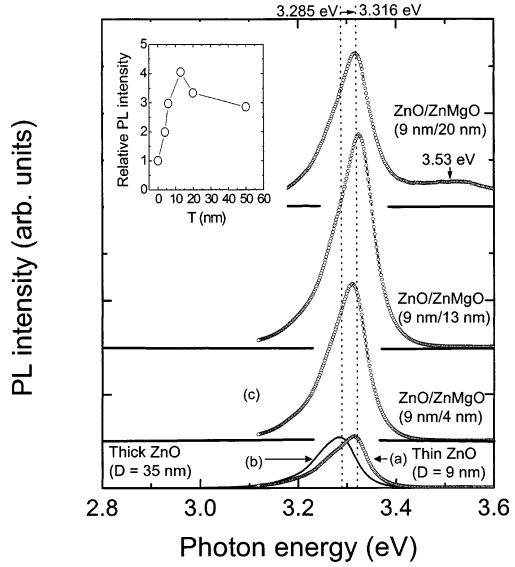

Figure 3. Room-temperature PL spectra of ZnO nanorods with average diameters of (a) 9 and (b) 35 nm, and (c) ZnO/$Zn_{0.8}Mg_{0.2}O$ coaxial nanorod heterostructures. The inset shows the normalized PL intensity of near-bandedge emissions, depending on the $Zn_{0.8}Mg_{0.2}O$ shell layer thickness.

heterostructures is allowed because of the negligible lattice mismatch (0.5%), consistent with the HR-TEM results.

Figure 3a−c shows room-temperature PL spectra of ZnO nanorods with average diameters of 9 and 35 nm and ZnO/$Zn_{0.8}Mg_{0.2}O$ coaxial nanorod heterostructures. As shown in Figure 3a,b, the dominant PL peak of ultrafine ZnO core nanorods with a diameter of 9 nm shows a 30 meV blue shift, compared with that of thick ZnO nanorods with a diameter of 35 nm due to the quantum confinement effect.[12] In addition, overall shape and dominant peak positions in the spectra from the thin ZnO nanorods are not significantly affected by the $Zn_{0.8}Mg_{0.2}O$ shell layer coating. In particular, the PL peak position of ZnO/$Zn_{0.8}Mg_{0.2}O$ coaxial nanorod heterostructures did not significantly depend on the thickness of the capping $Zn_{0.8}Mg_{0.2}O$ layer. However, for only the heterostructures with a $Zn_{0.8}Mg_{0.2}O$ shell layer thicker than 20 nm, a new emission peak was observed at 3.53 eV, corresponding to the near-bandedge emission of the $Zn_{0.8}Mg_{0.2}O$ layer. From all the above results, the possibility of alloy formation and the resulting blue shift of the PL peak can be ruled out, indicating that there is no significant intermediate layer formation in MOVPE growth of the coaxial nanorod heterostructures.

One of the significantly enhanced PL properties for coaxial nanorod heterostructures is much higher PL intensity than that of bare ZnO nanorods. As shown in the inset of Figure 3a, the integrated PL intensity of nanorod heterostructures increased with the $Zn_{0.8}Mg_{0.2}O$ layer thickness coating. This behavior is presumably related to surface state effects on radiative recombination of the coaxial nanorod heterostructures. In general, the surface acts like a defect and may induce nonradiative or radiative deep-level transitions. This surface effect is more serious for the thinner nanorods because of their higher surface/volume ratio. For the coaxial nanorod heterostructure, the $Zn_{0.8}Mg_{0.2}O$ shell layer can confine carriers in the ZnO core and hence suppress luminescent quenching by the surface state effect. In addition, the enhancement of the integrated PL intensity became higher with increasing $Zn_{0.8}Mg_{0.2}O$ layer thickness up to 13 nm, presumably because of the increased excitation volume for thicker nanorod heterostructures. However, further increases of shell layer thickness over 13 nm leads to a small decrease in the PL intensity. This may result from another radiative transition at 3.53 eV in $Zn_{0.8}Mg_{0.2}O$ or nonradiative transition by misfit dislocations. Dislocation density may start to increase significantly, as the shell layer thickness exceeds a certain critical thickness, thereby increasing the probability of carrier trapping to nonradiative recombination centers.

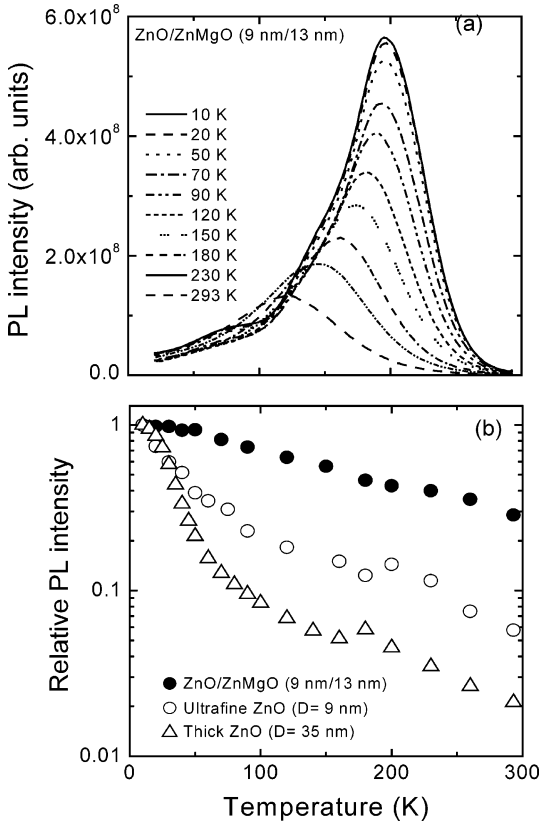

Figure 4. Temperature-dependent PL spectra of ZnO (9 nm diameter)/$Zn_{0.8}Mg_{0.2}O$ (13 nm thickness) nanorod heterostructures measured in the temperature range from 10 to 293 K. (b) Spectrally integrated PL intensity normalized with the PL intensity at 10 K as a function of temperature for thick (D = 35 nm) and ultrafine (D = 9 nm) ZnO nanorods and ZnO/$Zn_{0.8}Mg_{0.2}O$ coaxial nanorod heterostructures.

Further optical properties of ZnO/$Zn_{0.8}Mg_{0.2}O$ coaxial nanorod heterostructures were investigated by measuring their PL spectra at various temperatures between 10 K and room temperature. Figure 4a shows typical temperature-dependent PL spectra of ZnO (9 nm diameter)/$Zn_{0.8}Mg_{0.2}O$ (13 nm thickness) coaxial nanorod heterostructures. With increasing temperature, thermal quenching in the dominant PL peak was observed with a red shift of the dominant PL peak due to band gap shrinkage. For the coaxial nanorod heterostructures, however, thermal quenching is much lower than that of bare ZnO nanorods. From temperature-dependent integrated emission intensity for thick and ultrafine ZnO nanorods and the ZnO/$Zn_{0.8}Mg_{0.2}O$ coaxial nanorod heterostructures as shown in Figure 4b, the coaxial nanorod heterostructures exhibited the lowest thermal quenching. This results from reduced thermal escape to nonradiative centers, since radiative transition by electron and hole wave function overlap is enhanced because of carrier localization in the ultrafine ZnO nanorods and their coaxial heterostructures. Furthermore, the high-quality heteroepitaxial $Zn_{0.8}Mg_{0.2}O$ capping layer passivates surface nonradiative recombination centers, resulting in the reduced thermal quenching.[16,17]

Metal−organic vapor-phase epitaxy was used for fabrications of high-quality ZnO/$Zn_{1-x}Mg_xO$ coaxial nanorod heterostructures with abrupt interfaces. TEM revealed a defect-free, clean

interface between ZnO and $Zn_{0.8}Mg_{0.2}O$ layers, and their PL spectra also exhibited a blue shift in the PL peak position, significantly increased PL intensity, and notably reduced thermal quenching, presumably resulting from the quantum effect. Our controlled heteroepitaxial growth of coaxial nanorod heterostructures opens up significant opportunities for fabrication of nanorod device structures with radial composition modulation. In particular, these coaxial nanorod heterostructures may be very useful for high-efficiency light-emitting device applications.

Acknowledgment. This work was financially supported through the National Creative Research Initiative Project by the KOSEF and the Air Force Office of Scientific Research (AOARD-054084), U.S.A.

References and Notes

(1) Park, W. I.; Yi, G.-C.; Kim, M.; Pennycook, S. J. *Adv. Mater.* **2003**, *15*, 526.

(2) Björk, M. T.; Ohlsson, B. J.; Thelander, C.; Persson, A. I.; Deppert, K.; Wallenberg, L. R.; Samuelson, L. *Appl. Phys. Lett.* **2002**, *81*, 4458.

(3) Gudiksen, M. S.; Lauhon, L. J.; Wang, J.; Smith, D. C.; Lieber, C. M. *Nature (London)* **2002**, *415*, 617.

(4) Wu, Y.; Fan, R.; Yang, P. *Nano Lett.* **2002**, *2*, 83.

(5) Wu, Y.; Xiang, J.; Yang, C.; Lu, W.; Lieber, C. M. *Nature (London)* **2004**, *430*, 61.

(6) Lin, H.-M.; Chen, Y.-L.; Yang, J.; Liu, Y.-C.; Yin, K.-M.; Kai, J.-J.; Chen, F.-R.; Chen, L.-C.; Chen, Y.-F.; Chen, C.-C. *Nano Lett.* **2003**, *3*, 537.

(7) Lauhon, L. J.; Gudiksen, M. S.; Wang, D.; Lieber, C. M. *Nature (London)* **2002**, *420*, 57.

(8) Tsang, W. T. *Semiconductors and Semimetals*; Willardson, R. K., Beer, A. C., Eds.; Academic Press: San Diego, 1987; Vol 24, pp 397−458.

(9) Choi, H.; Johnson, J.; He, R.; Lee, S.; Kim, F.; Pauzauskie, P.; Goldberger, J.; Saykally, R.; Yang, P. *J. Phys. Chem. B* **2003**, *107*, 8721.

(10) Heo, Y. W.; Kaufman, M.; Pruessner, K.; Siebein, K. N.; Norton, D. P.; Ren, F. *Appl. Phys. A* **2005**, *80*, 263.

(11) Razeghi, M. *The MOCVD challenge*; Adam Hilger: Bristol, 1989.

(12) Park, W. I.; Yoo, J.; Yi, G.-C. *J. Korean Phys. Soc.* **2005**, *46*, L1067.

(13) Jung, S. W.; Park, W. I.; Cheong, H. D.; Yi, G.-C.; Jang, H. M.; Hong, S.; Joo, T. *Appl. Phys. Lett.* **2002**, *80*, 1924.

(14) An, S. J.; Park, W. I.; Yi, G.-C.; Kim, Y.-J.; Kang, H. B.; Kim, M. *Appl. Phys. Lett.* **2004**, *84*, 3612.

(15) Kim, M.; Yi, G.-C.; Kong, K. J.; Chang, H.; Yoo, J.; Park, W. I.; Park, G.-S.; Pantelides, S. T.; Pennycook, S. J. Submitted for publication.

(16) Cao, Y.-W.; Banin, U. *Angew. Chem., Int. Ed. Engl.* **1993**, *32*, 3692.

(17) Dabbousi, B. O.; Rodriguez-Viejo, J.; Mikulec, F. V.; Heine, J. R.; Mattoussi, H.; Ober, R.; Jensen, K. F.; Bawendi, M. G. *J. Phys. Chem B* **1997**, *101*, 9463.